Parameter Importance in FRAP Acquisition and Analysis: A Simulation Approach

Juliane Mai,[†*] Saskia Trump,[‡] Irina Lehmann,[‡] and Sabine Attinger[†§]
[†]Department of Computational Hydrosystems and [‡]Department of Environmental Immunology, Helmholtz Centre for Environmental Research, Leipzig, Germany; and [§]Institute for Geosciences, University of Jena, Jena, Germany

ABSTRACT Fluorescence recovery after photobleaching (FRAP) is a widespread technique used to determine intracellular reaction and diffusion parameters. In recent years, due to technical advances and an increasing number of mathematical models for analysis, there was a resurging interest in FRAP applications. However, care has to be taken when inverting parameters from such data. We study potential influences on FRAP acquisition and analysis like initial fluorescence distribution, membrane passage, and geometrical aspects. Monte Carlo simulations are employed for the investigation of reaction-diffusion processes to additionally include cases in which no analytical description is available. To assess the importance of influencing factors we apply a sensitivity method based on elementary effects providing an estimate for the global parameter space. The combination of simulations and sensitivity measure helps us to predict ranges of parameters used in acquisition and analysis for which a reliably inversion of reaction-diffusion parameters is possible. Using this approach, we show that FRAP data are highly susceptible to misinterpretation. However, by identifying the parameters of susceptibility, our analysis provides the means for taking measures to significantly improve FRAP data interpretation and analysis.

INTRODUCTION

The interest in molecular interaction and dynamics in living cells is steadily increasing. Several experimental approaches based on fluorescent microscopy have been developed over the years. One of the most widespread techniques to investigate molecular mobility in living cells is fluorescence recovery after photobleaching (FRAP) (1–9).

The underlying strategy of a FRAP experiment is quite simple. A region of interest (ROI) is chosen and the fluorescence in this area is irreversibly bleached by a laser beam. Subsequently, the reoccurrence of the fluorescence in the ROI is monitored over time, giving rise to a so-called recovery curve. The shape of this curve is determined by the characteristics of mobility, e.g., molecular interaction, diffusion, or directed movement. Therefore, FRAP experiments can be used to deduce parameters characterizing processes such as diffusion coefficients or reaction rates (10–15).

Due to the implementation of FRAP acquisition tools on commercially available microscopes, and the introduction of fluorescent proteins like GFP, the interest in FRAP applications experienced a resurge in recent years. Despite these technical advances and an increasing number of mathematical models for analysis (16–18), some considerations are still warranted when inverting parameters from such experiments. Not only the experimental setup, but also the subsequent mathematical analysis of the generated FRAP data, can have a marked effect on the parameter outcome. In this respect, we evaluated the importance of FRAP acquisition and analysis parameters, employing Monte Carlo simulations coupled with a sensitivity measure.

Simulations (i.e., numerical models) can facilitate the understanding of cellular systems in particular if spatio-temporal parameters take on importance. Evaluating which model parameters are most influential and which are negligible can provide further insight into the system investigated. However, for a comprehensive model assessment, the overall impact of all parameters on the model output should be determined by using as small a number of model evaluations as possible. Several methods are available for such a sensitivity analysis to provide a quantitative measure of the parameter importance. These methods differ in complexity and in the parameter information generated (19). Methods used to determine the influence of a single parameter on the model response while neglecting interaction between parameters are known as screening methods. These are based on sampling. Parameter sets are sampled from a distribution and used subsequently to drive the model.

One particularly useful screening method for computationally expensive models is based on elementary effects, because this approach only needs a small number of model evaluations to determine a sensitivity measure for each parameter. The concept of the elementary effects method was introduced by Morris (16). A derivative choosing the parameter sets such that the complete feasible domain of parameter values is covered was introduced by Saltelli et al. (17). We used this approach to determine the importance of parameters used in acquisition and analysis of FRAP.

Numerical models are computationally very expansive, therefore the reaction-diffusion parameter inversion from FRAP data commonly relies on simplified analytical models. These simplifications are based on assumptions that usually do not hold in the environment of a living cell. It is easy to imagine that, by these model assumptions,

Submitted July 25, 2012, and accepted for publication March 1, 2013.

*Correspondence: juliane.mai@ufz.de

Editor: Michael Stern.

0006-3495/13/05/2089/9 $2.00

http://dx.doi.org/10.1016/j.bpj.2013.03.036

only approximate model functions describing the time course of the fluorescence recovery within the ROI can be deduced, which will lead to inaccurate parameter values (i.e., diffusion coefficients and reactions rates).

In this article, the influence of these model assumptions as well as the influence of the experimental setup (e.g., the position of the bleaching spot, and the geometry of the bleached compartment) will be studied.

We will show that FRAP experiments are highly susceptible to misinterpretation. A prerequisite for the successful combination of biological observations with mathematical models is an accurate data acquisition as well as an appropriate model assumption set. Therefore, it seems evident to use simulations of FRAP measurements in combination with a sensitivity measure to determine the main influencing factors on FRAP recovery curves to significantly improve their interpretation and analysis.

SIMULATIONS AND SENSITIVITY ANALYSIS

To determine possible influencing factors of FRAP experiments, we use a simulation framework of such experiments as well as a strategy to quantitatively determine the impact of each of these factors.

We start out by describing our general setup of FRAP simulations. Subsequent to the verification of the simulator, we investigate the impact of different experimental and analytical aspects of a FRAP experiment. To gain a quantitative measure, we apply a sensitivity method allowing a direct comparison of various influencing factors on the output of a FRAP experiment.

Simulations

FRAP data reflect intracellular spatio-temporal processes. The mathematical description of these processes necessitates partial differential equations (PDEs). Such PDEs consist of four different components:

1. Spatio-temporal processes.
2. Initial conditions.
3. Boundary conditions.
4. The feasible domain.

Therefore, our FRAP simulator integrates:

Processes

The most important intracellular molecular processes that have to be addressed are movement and interaction. Our simulator considers reaction and diffusion. Although advection would be a special case covered by our simulation framework, it was not further investigated.

Initial conditions

In general, the initial condition describes the characteristics of the modeled system at time step $t = 0$. Specifically, for FRAP simulations, the experimentally observed fluorescence distribution immediately after bleaching has to be approximated. Different types of such approximations are considered.

Boundary conditions

The boundary condition specifies the behavior of the modeled system at the boundaries of the geometries. Regarding fluorescent particles, the boundary condition specifies, e.g., a possible passage over a membrane.

Geometry of the feasible domain

The cellular space in which the experiment is performed has to be taken into account. Corresponding geometries can be simplified, or real cell geometries can be used.

The explicit system of PDEs for $(S + 1)$ diffusing and reactively coupled compounds B_i is given in Eq. 1, where D_{B_i}, k_{on_i}, and k_{off_i} are the diffusion coefficients and the association and dissociation rate of the compound B_i, respectively. The initial as well as the boundary conditions have to be chosen corresponding to the application examples given in Mai et al. (18):

$$\frac{dc_{B_0}}{dt} = D_{B_0}\nabla^2 c_{B_0} - k_{on_1} c_{B_0} + k_{off_1} c_{B_1}, \tag{1a}$$

$$\frac{dc_{B_i}}{dt} = D_{B_i}\nabla^2 c_{B_i} + k_{on_i} c_{B_{i-1}} - k_{off_i} c_{B_i} - k_{on_{i+1}} c_{B_i} + k_{off_{i+1}} c_{B_{i+1}},\ i = 1 \ldots S-1, \tag{1b}$$

$$\frac{dc_{B_S}}{dt} = D_{B_S}\nabla^2 c_{B_S} + k_{on_S} c_{B_{S-1}} - k_{off_S} c_{B_S}. \tag{1c}$$

The detailed specifications of the implementation of the above-mentioned processes and methods can be found in the Supporting Material, including excerpts of the source code.

Numerical implementation

We employed Monte Carlo simulations to solve our numerical models and define their realizations as particles, although they do not have a spatial dimension. The advantage of these Monte Carlo simulations is that only the boundaries of the simulation domain (in our case plasma or nuclear membrane) have to be discretized, and no mesh of the whole domain has to be generated.

Discretization

To assure comparability of the simulation results we chose a standardized simulations setup.

Simulations were performed using 1000 time steps, 10,000 particles, and a time discretization of $\Delta t = 0.005$. To achieve a smooth recovery curve, 10 simulations per model and parameter set were averaged. These averaged

curves were then compared with either the analytical solutions or, where applicable, the simulation results.

Simulations of two reactively coupled, diffusing particle types were performed. Parameter ranges for reaction and diffusion were chosen corresponding to the literature (18–20) and can be found in Table 1.

The overall number of simulations depended on the amount of parameters studied and was set according to the Morris method (see Section S2.3 in the Supporting Material).

Code verification

The performance of all algorithms implemented for the particle-based simulations had to be confirmed. Therefore, we employed analytical solutions of reaction-diffusion problems as described in Mai et al. (18) and compared them with simulations of such experiments under the same conditions used for calculating the analytical solutions. The models used include multiple diffusion and reaction schemes (see Section S3 in the Supporting Material).

We demonstrate exemplarily the results for two different model types:

1. Diffusion of only one fraction of reactively coupled particles while the other fraction is immobile; and
2. Diffusion of both particle fractions (Fig. 1).

The initial bleaching profile applied corresponds to the adapted constant initial condition (see Section S3.1 in the Supporting Material). For both models an analytical solution has been described previously (18).

Sensitivity analysis

The results of simulations using the previously described implementations, are strongly dependent on the parameterization of the processes, i.e., the result will change by variation of diffusion coefficients or the simulation domain. The following section will describe the elementary effects-based method we used to quantify these changes allowing for a comparability of parameter impacts.

TABLE 1 Reaction-diffusion parameter values and ranges

	D_1	D_2	k_{on}	k_{off}
I_A	10	1	0.5	0.5
I_B	[5, 10]	[0, 5]	[0.001, 1]	[0.001, 1]
II_{A1}	10	1	0.5	0.5
II_{A2}	10	1	0.5	0.5
II_{B1}	[5, 10]	[0, 5]	[0.001, 1]	[0.001, 1]
II_{B2}	[5, 10]	[0, 5]	[0.001, 1]	[0.001, 1]
III_{A1}	10	1	0.3	0.05
III_{A2}	10	1	0.3	0.05
III_{A3}	10	1	0.3	0.05
III_{A4}	10	1	0.3	0.05
III_B	[5, 10]	[0, 5]	[0.001, 1]	[0.001, 1]

Reaction-diffusion parameter values and ranges used for Monte Carlo simulations. Two reactively coupled, diffusing particle types are simulated. The diffusion coefficients are D_1 and D_2 whereas the reaction is determined by the association and dissociation rates k_{on} and k_{off}, respectively.

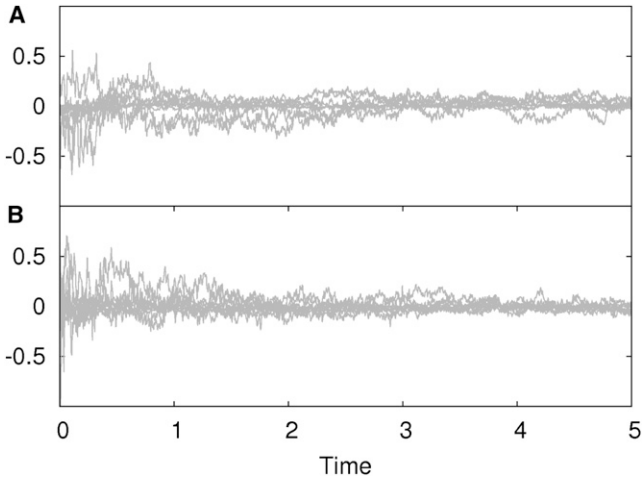

FIGURE 1 Analysis of simulation accuracy. Relative error between FRAP simulations and analytical solutions. Each subplot shows the error at each simulated time step using 10 different parameter sets. (*A*) Simulation of two reactively coupled particle fractions, one diffusing and the other one immobile. (*B*) Both reactively coupled particle fractions are diffusing.

In general, an elementary effect is the change of the model output given by adjusting one parameter whereas all others kept constant. It is defined as

$$EE_i = \frac{M(p_1, p_2, \ldots, p_i+\Delta, \ldots, p_N) - M(p_1, p_2, \ldots, p_i, \ldots, p_N)}{\Delta}, \tag{2}$$

where EE_i is the elementary effect of the ith parameter, M is the model dependent on the N parameters $p_1,\ldots,p_N$, and Δ is the change of the ith parameter. The parameters have to be scaled to the unit interval [0,1], because the scaling of the parameter to true values is already a part of the model. Therefore, Δ will also range between 0 and 1.

To obtain the elementary effect of a certain parameter i, the EE_i has to be calculated for K different parameter constellations to assure a mean effect of this parameter i. An overall number of $2NK$ parameter sets would be necessary to estimate the elementary effect of the N parameters based on K single samples (NK reference sets and NK sets with adjusted parameter values). In turn, $2NK$ model runs are needed to calculate the elementary effects. To reduce the number of parameter sets and therefore the number of model runs, an efficient way to sample is the use of K parameter trajectories.

A parameter trajectory is generated as follows:

(A) A permutation of the vector $m = (1,2,\ldots,N)$ is calculated;
(B) A random, initial parameter set $p^{(0)}$ is generated;
(C_1) The second parameter set $p^{(1)}$ is determined by $p^{(0)}$, with the parameter corresponding to the first entry of m adjusted;

(C_2) The next parameter set $p^{(2)}$ is determined by $p^{(1)}$, with the parameter corresponding to the second entry of m adjusted; and

(C_N) The last parameter set of the trajectory $p^{(N)}$ is determined by $p^{(N-1)}$, with the parameter corresponding to the last entry of m adjusted.

By using this parameter sampling strategy, the number of parameter sets in use is reduced from $2NK$ to $(N + 1)K$. This design was suggested by Morris (16).

For generating the trajectories, a MATLAB (Ver. 2012a, The MathWorks, Natick, MA) code was employed from the MATLAB Toolbox (21).

The proper elementary effect per parameter is calculated subsequently based on K single values. Because the mean of the values μ_i may prove misleading due to cancellation of effects (22), it is suggested to use the mean of the absolute single values,

$$\mu_i^* = \frac{1}{K}\sum_{j=1}^{K}\left|EE_i^{(j)}\right|, \tag{3}$$

where K is the number of trajectories and $EE_i^{(j)}$ is the elementary effect of parameter i within the jth trajectory, and μ_i^* is the sensitivity measure of the ith parameter.

We used $K = 20N$ trajectories in all of our elementary effect studies. Therefore, the total number of parameter sets equals $20N\ (N + 1)$.

ANALYSIS OF FRAP MODELING AND ACQUISITION

The performance of the simulations was tested successfully against our recently described analytical solution of the FRAP recovery curve (18). In all simulations performed the relative error between simulation and analytical solution was randomly distributed around zero and below 0.5% (see Fig. 1), demonstrating the reliable performance of the implemented algorithms. The same was observed for all other models (described in Mai et al. (18)), reaction schemes, initial conditions, and parameter sets (data not shown).

Because modeling assumptions are often only simplifications of the reality, we determined the impact of variations in these assumptions by varying corresponding model parameters. The model parameters were adapted by using the Morris method. The elementary effects were then calculated to gain a sensitivity measure.

The following three conditions were investigated in detail:

1. Initial condition. What is the most appropriate model description for the fluorescence distribution immediately after the bleach? We addressed the question which of the simplified initial distributions describes the Gaussian profile best, and whether this simplification can be generalized (i.e., for arbitrary reaction diffusion parameters).
2. Boundary condition. Do we need to restrict movement possibilities of the fluorophores in our models? To study this issue in more detail, we investigated the influence of the chosen boundary condition on the parameter inversion outcome.
3. Geometry. It seems likely that the geometry of the bleached compartment has a considerable impact on inverted parameters. As a generalized approach, we sampled the whole parameter space using real cell geometries as a bleaching compartment.

Other factors are also known to influence the analysis and acquisition of FRAP data (23–28). Two of these cases considering normal diffusion, while neglecting sub- or superdiffusion and the simplification of three-dimensional processes by two-dimensional projections, were investigated in addition to Conditions 1–3. Corresponding results can be found in the Supporting Material. In contrast to the simplification of anomalous diffusion we employed, many studies have investigated the influence of internal boundaries in a more explicit way by using geometries of real cellular structures extracted from microscopy or tomography data (25,26,29). In this study, we focus on the general impact of sub- and superdiffusion. Whereas our approach can also be extended to determine the impact of real cellular boundaries, the simplified strategy will yield a reliable approximation of the general impact of heterogeneous environments.

Using FRAP simulations, we aim to identify the most influential (i.e., sensitive) factors on the outcome of a FRAP experiment. These results are essential for an optimized experimental setup and for assessing whether determined reaction diffusion parameters are reliable.

Influence of initial distribution inside the bleaching spot

The bleaching spot profile observed directly after bleaching corresponds to a Gaussian distribution, which cannot be described analytically in most cases. Nevertheless, methods have been described of how to adapt the initial Gaussian condition to make calculating an analytical solution possible. The initial fluorescence intensity profile in the bleaching spot is simplified either by a constant or adjusted constant (19) bleaching profile, or, in the most simplified way, the initial fluorescence intensity (I_0) is considered to be $I_0 = 0$ (10). We investigated whether these different initial conditions (ICs) are an appropriate approximation of the initial fluorescence distribution.

We started by using the specific parameter set I_A (Tables 1 and 2) for the comparison of three different initial conditions as depicted in Fig. 2. These values were used to adjust the initial value θ and the radius R (see the Supporting Material for a detailed description). Simulations with these particular parameters led to a recovery adequately

TABLE 2 Experimental parameter values and ranges

	Bleaching spot (a, σ, r_0) or (θ, r)	Position spot (d, R) or (d_M)	b
I_A	0.8, 1.2, 1	—	—
I_B	[0.1, 0.9], [0.1, 2], [0.5, 2.5]	—	—
II_{A1}	0.1, 2	1.8, 4	0
II_{A2}	0.1, 2	1.8, 4	1
II_{B1}	[0.1, 0.9], [0.1, 0.9]	[0, 3], [4, 10]	[0, 1]
II_{B2}	[0.55, 0.71], [1.74, 2.18]	[0, 3], [4, 10]	[0, 1]
III_{A1}	0.1, 1	14.23	0
III_{A2}	0.1, 1	8.64	0
III_{A3}	0.1, 1	12.69	0
III_{A4}	0.1, 1	6.05	0
III_B	[0.55, 0.71], [1.74, 2.18]	[7.5, 14.25]	0

Experimental parameter values and ranges used for Monte Carlo simulations. For bleaching profile, either a Gaussian distribution is chosen (bleaching level a, standard deviation σ, and radius r_0) or an adjusted constant profile (bleaching level θ and adjusted radius r) is chosen. The position of the bleaching spot is specified by the distance between the center of the bleaching spot and a circular compartment d and a radius R of this circular compartment or a mean (average) distance to a complex compartment geometry d_M. The kind of boundary condition is set by b.

approximating the curve of the Gaussian IC only if an adjusted constant initial value θ (adapted radius R) were used, while the constant IC led to pronounced discrepancies between the recovery curves (Fig. 2). To prove that these results are not only valid for this specific parameter set, the elementary effects were calculated for all the reaction-diffusion and experimental setup parameters (parameter ranges used for simulation are I_B; see Tables 1 and 2).

A total of 1120 ($= 20\,N(N+1)$) parameter sets were used to simulate FRAP curves considering all four different ICs (Gaussian profile, zero initial profile, constant profile, and adjusted constant profile). The elementary effects were calculated as differences to the Gaussian IC and were used to identify the parameters responsible for the deviation. The results as depicted in Fig. 3 show that the adjusted constant IC performs best over the whole parameter range, suggesting that it represents the most appropriate simplification of the initial bleaching profile. The elementary effects of the other two ICs are significantly larger for all parameters investigated.

Interestingly, the most sensitive parameters of the adjusted constant IC are the experimental parameters a and σ describing the characteristics of the Gaussian profile (i.e., depth a and variance σ). Consequently, it should be taking care of a comparable bleaching profile over all FRAP experiments analyzed.

Our simulations showed that an adjusted constant IC with the corresponding analytical solution is an appropriate approximation of the initial Gaussian distribution.

Influence of boundary condition

In typical FRAP models, the bleached compartment is considered to be infinite, allowing the observed molecules to distribute evenly across all membranes (boundary). This flow boundary condition usually does not apply to real cellular environments.

That the boundary condition indeed has an impact on the model outcome has already been shown (12,30) for selected parameter sets. However, to determine whether this is a general effect over different parameter ranges, we performed simulations using different boundary conditions and determined their effect on the parameter inversion outcome.

We started by running simulations with specific parameter sets II_{A1} and II_{A2} (Tables 1 and 2) in an artificial

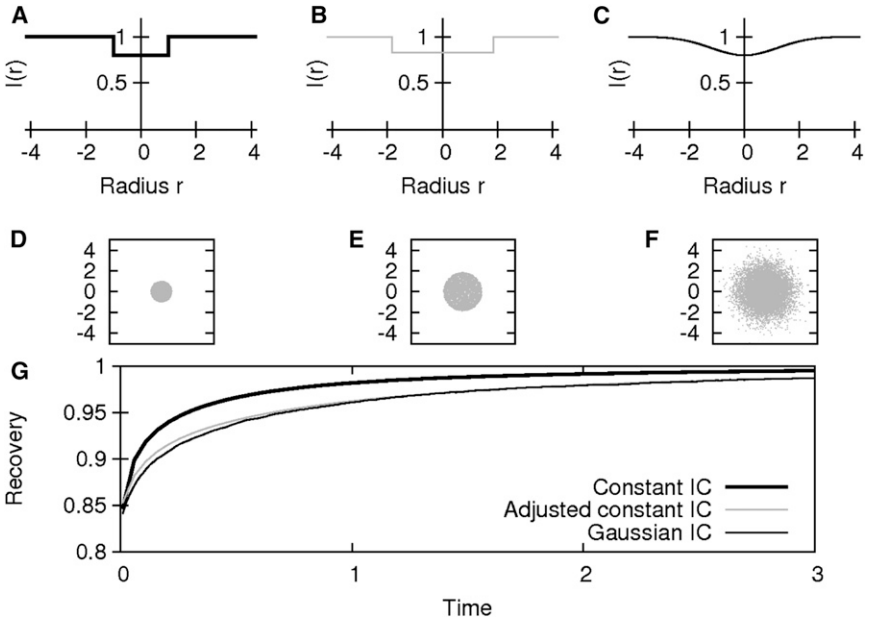

FIGURE 2 Influence of different types of initial condition (IC). (*A–C*) Bleaching spot profiles. (*D–F*) Initial distribution of bleached particles. (*A* and *D*) Constant IC. (*B* and *E*) Adjusted constant IC. (*C* and *F*) Gaussian IC using parameter set (I_A), and (*G*) resulting FRAP recovery curves.

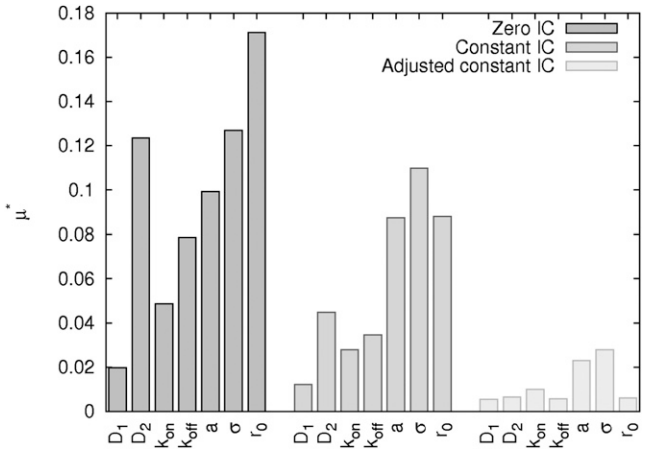

FIGURE 3 Influence of different parameters on mean absolute error between Gaussian IC versus simplified ICs. Elementary effects μ^* of reaction-diffusion parameters (D_1, D_2, k_{on}, k_{off}) and the experimental setup (depth a and variance σ of Gaussian profile and radius of spot r_0) using parameter ranges (I_B).

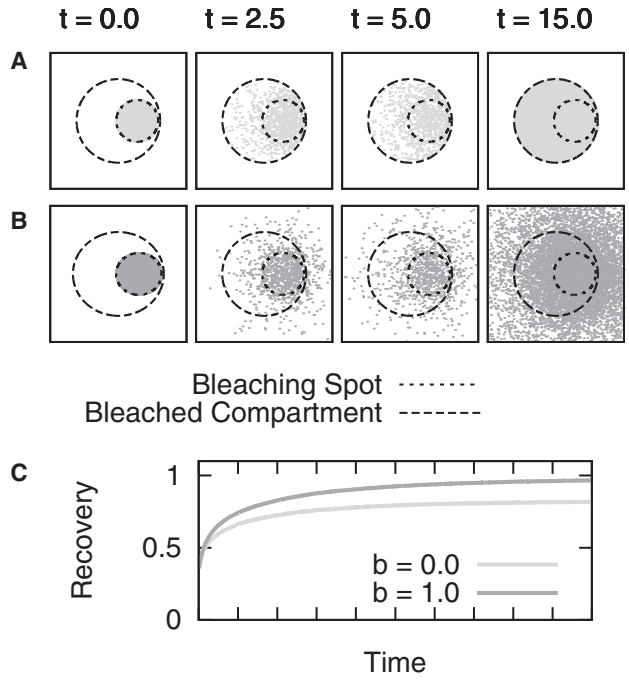

FIGURE 4 Influence of the chosen boundary condition on the FRAP recovery curve. Results are shown for simulations in a circular geometry with a bleaching spot positioned at the edge of the domain. (*A*, *upper panel*) Distributions of bleached particles considering a no-flow boundary are depicted (parameter set II_{A1}). (*B*, *lower panel*) Here, the no-flow boundary condition was omitted (parameter set II_{A2}). (*C*) Corresponding recovery curves.

geometry. A circular geometry, exemplifying an arbitrary membrane enclosed cellular structure, was used as a simulation domain with either a flow boundary condition ($b = 1$; i.e., particles are allowed to cross the membrane without hindrance), or with a no-flow boundary condition ($b = 0$; i.e., the particles are restricted to the membrane enclosed domain).

The final distribution of particles simulated and the resulting averaged recovery curves are depicted in Fig. 4. It seems obvious that the simulations using this specific parameter set attach great importance to the boundary condition chosen.

The elementary effects were determined to assess whether or not this is a general outcome. All simulations were run employing the adjusted initial condition as we showed it to be the most appropriate approximation of the Gaussian profile. The parameter ranges used for the Monte Carlo simulations are II_{B1} (Tables 1 and 2).

A total of 1800 ($= 20\,N\,(N+1)$) parameter sets were used to simulate the according FRAP curves and calculate the elementary effects based on the absolute distance between two recovery curves. The results as shown in Fig. 5 (*black bars*) are particularly interesting in two aspects: The most sensitive factors are θ and r describing the initial profile while b, the parameter characterizing the probability of particles crossing a boundary, is highly insensitive.

We wondered whether the insensitivity of b might be due to the broad range for θ and r chosen for the previous elementary effect analysis. We already learned while studying the influence on the initial condition that the initial profile should be kept constant during the experiments. Therefore, we restricted the range of θ and r to values obtained in real FRAP experiments (AhR-GFP bleached within the cytoplasm of Hepa-1c1c7 cells; see parameter ranges II_{B2} in Tables 1 and 2). Simulations were run again with 1800 parameter sets where only the values of θ and r were adapted according to the restricted parameter ranges. Simulation results are depicted in Fig. 5 (*gray bars*). Limiting the parameter ranges of θ and r has no effect on the elementary effect of b.

Although our initial simulation using a single specific parameter set alleges an important role of the boundary condition chosen, our global analysis of arbitrary and experimental parameter ranges disproves this observation. In conclusion, these findings suggest that the boundary condition chosen has only a marginal effect on the inverted reaction diffusion parameters. Furthermore, inversion of a fast diffusion coefficient (D_1) is highly unreliable, because the experimental parameters (θ and r) are more sensitive and therefore have an even greater impact on the FRAP recovery curve than the parameter of interest. The goal would be to decrease the ranges of the experimental parameters until their elementary effect is lower than that of each reaction-diffusion parameter.

Influence of bleaching spot position

In a setup similar to that described above for the boundary condition, the significance of the bleaching spot position for the FRAP recovery outcome was assessed. A cytoplasmic geometry was reconstructed from microscopy

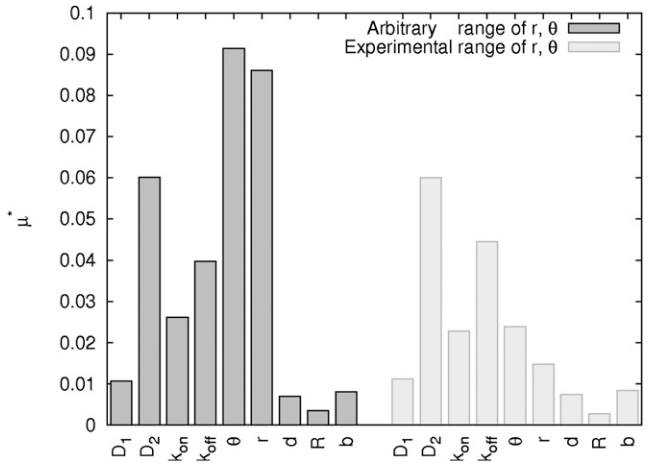

FIGURE 5 Effect of boundary condition. Elementary effects μ^* of reaction-diffusion parameters (D_1, D_2, k_{on}, k_{off}) and experimental setup: depth θ and adjusted radius r of bleaching spot, distance between center compartment and center spot d, radius R of circular compartment and probability allowing particles crossing the membrane b (parameter ranges II_{B1} and II_{B2}).

images using NeuRA2 (31,32) and simulations were performed at four different bleaching spot positions using 400 time steps to simulate 20 time units (Fig. 6 *A*). Recoveries of two different fractions of particles were examined using the parameterization III_A (Tables 1 and 2).

To find a reference recovery curve for comparison, we studied the particle distribution within the geometry at the simulated time steps (see the Supporting Material). A homogeneous distribution of particles was only observed for the central position of the bleaching spot (Fig. 6, *Spot 1*). Therefore, the corresponding recovery curve was set as a reference.

In these four examples, an influence of the bleaching spot position on the recovery curve is only apparent in regions of hindered diffusion (Fig. 6, *Spots 2* and *4*). Interestingly, a position next to the boundary of the geometry where the diffusion can take place unhindered to at least one half-plane (Fig. 6, *Spot 3*) has only a negligible influence on the recovery curve. We can then conclude that bleaching spots should not be positioned in regions like the cell edge, where protrusions could restrict the diffusion.

To prove that these observations are true not only for the single specific setup just presented but for the whole parameter range, the elementary effects were determined. Our previous results made obvious that the variations in experimental parameters should be minimized. Therefore, simulations were performed with limited, experimentally deduced, parameter ranges for r and θ (parameter ranges III_B, Tables 1 and 2) to reliably assess the sensitivity of the reaction-diffusion parameters related to the bleaching spot position.

To address the relative position of the bleaching spot to the compartment boundary, we introduce a new parameter d_M, which represents the mean distance to the periphery. The value d_M is calculated as the mean length of 60 line segments from the bleaching spot center to the geometry boundary. This distance measure yields small values for positions in protrusions of a geometry and comparatively large values for those near a half-plane (Fig. 6, *Spot 3*) and in the center of the geometry (Fig. 6, *Spot 1*). The distribution of the distance-measure d_M within the cytoplasmic geometry can be found in the Supporting Material. The parameter d_M was varied in a range according to its distribution. A total of 1120 parameter sets ($= 20\,N\,(N+1)$) were used to simulate the according FRAP curves and calculate the elementary effects based on the absolute distance between two curves.

The analysis showed that d_M does have a significant impact on the recovery—one that is even higher than that of the other experimental parameters (θ, r). Because the sensitivity of a parameter is directly related to the corresponding parameter range, limiting this range increases parameter certainty (see Section S3.2 in the Supporting Material). Therefore, the variation of d_M has to be narrowed to achieve the overall goal of a reliable parameter inversion for diffusion and reaction processes. Although this seems hard to accomplish, large variations of d_M can only appear if spot positions in diverse parts of the geometry are used for the bleaching experiments. Performing the experiments in comparable regions of the geometry is particularly important, as it is hard to calculate the uncertainty (i.e., parameter range) of this parameter in retrospect; information about the relative position of the bleaching spot and the cellular boundaries is limited.

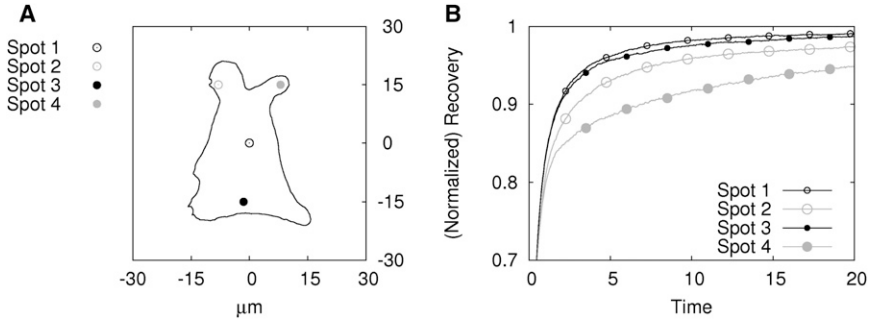

FIGURE 6 Influence of the bleaching spot location on the FRAP recovery. (*A*) Cytoplasmic geometry with four different positions of the bleaching spot. (*B*) Simulation results (recovery curves; parameter sets III_A).

DISCUSSION

Intracellular reaction-diffusion parameters are commonly inverted from FRAP data. Although performing such experiments is facilitated by implementation of FRAP acquisition tools on commercially available microscopes, some aspects still have to be considered. Either the experimental setup or the subsequent analysis can contribute to misleading data interpretation, which has already been shown by several groups (19,23–26,30). All these studies focused on specific parameter sets. However, we propose a global approach employing Monte Carlo-based reaction-diffusion simulations coupled with a sensitivity measure based on elementary effects. Calculating elementary effects allows us to deduce the general influence of a parameter, obviating a bias by choosing a nonrepresentative parameter set.

The initial condition (IC), i.e., the initial fluorescence distribution characterized by the depth and the width of the Gaussian profile, was identified as a main influencing factor on the shape of the recovery curve. Variations in this initial distribution led to an uncertainty in reaction-diffusion parameter inversion. This issue can be addressed first of all by using identical settings in a set of FRAP experiments, which is usually taking care of. However, even accurate data acquisition can lead to diverse bleaching profiles. Concluding from our study an a posteriori outlier selection would be advisable to assure the comparability of the initial fluorescence distribution.

Because an analytical solution is not available for a Gaussian initial profile, parameter inversion models rely on an approximated IC. Our comparison showed that the adjusted constant IC is not only an adequate approximation of the Gaussian profile but also outperformed all other available ICs.

Although in cellular systems various mechanisms of membrane transport exist (i.e., boundary conditions of the system), analytical models used for parameter inversion of FRAP data only consider unhindered membrane passage. Unexpectedly, variations in transport mechanism indeed only had a minor impact on the recovery curve, indicating that such models can be used for data analysis without concern.

Cellular geometries can be very diverse with respect to the domain available for an unhindered diffusion. Therefore, positioning of the bleaching spot might have an considerable impact on the FRAP recovery. Our simulations showed that only in exceptional cases, like bleaching in cell edge protrusions, the spot position has a perceivable influence. Nevertheless, such positions should be avoided during data acquisition—especially because it is not possible to retrace the position of the bleaching spot relative to the compartment geometry from the generated imaging data. Hence, an a posteriori outlier selection cannot be performed as proposed for the initial distribution. Neglecting a priori considerations for bleaching spot positioning would increase the parameter uncertainty.

Overall, the parameters describing the initial bleaching profile, i.e., the bleaching efficiency and the size of the bleached region, were among the most sensitive factors in all cases investigated (Fig. 7). This underlines the importance of a consistent experimental setup together with an a posteriori selection of inconsistent measurements. Apart from these experimental aspects, a bleaching spot position avoiding cell protrusions is recommended. Surprisingly, our study showed that an exact knowledge of the underlying membrane transport mechanisms is not essential for an accurate data analysis.

In conclusion, our work shows that elementary effects are a valuable tool in assessing parameter influences. We demonstrate that using only specific parameter sets can lead to contradictory results compared to the global elementary effects. Therefore, conducting a sensitivity analysis is highly valuable not only in studying FRAP data but also in studying intracellular processes in general.

SUPPORTING MATERIAL

Additional Information on Implementation of Reaction, Diffusion, Initial, and Boundary Conditions as well as Influence of bleaching spot position, Sub-/Super-Diffusion, and Projection Errors of 3D Processes are available at http://www.biophysj.org/biophysj/supplemental/S0006-3495(13)00375-5.

We are deeply indebted to Matthias Cuntz (Helmholtz Centre for Environmental Research, Leipzig, Germany) for critical comments and helpful discussion.

J.M. was supported by the Helmholtz Impulse and Networking Fund through the Helmholtz Interdisciplinary Graduate School for Environmental Research (HIGRADE). Note that this publication was based on studies performed as part of our project “From Contaminant Molecules

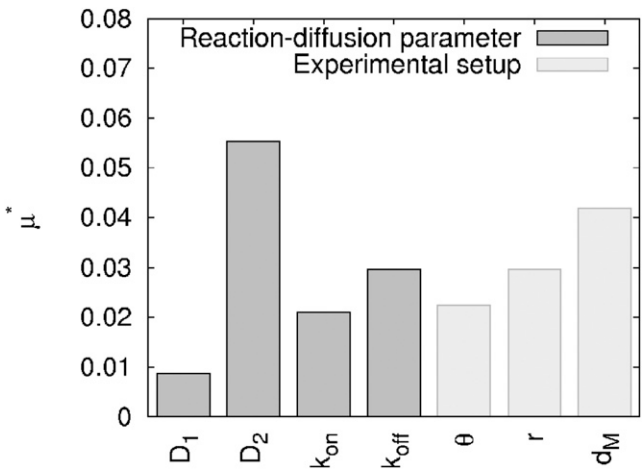

FIGURE 7 Effect of bleaching spot position. Elementary effects μ^* of reaction-diffusion parameters (D_1, D_2, k_{on}, k_{off}) and experimental setup (depth θ and adjusted radius r of bleaching spot as well as median distance d_M of bleaching spot center to compartment's boundary) in real geometry (parameter ranges III_B).

to Cellular Response: System Quantification and Predictive Model Development", which was funded by the Helmholtz Alliance on Systems Biology.

REFERENCES

1. Phair, R. D., S. A. Gorski, and T. Misteli. 2004. Measurement of dynamic protein binding to chromatin in vivo, using photobleaching microscopy. *Methods Enzymol.* 375:393–414.
2. Phair, R. D., P. Scaffidi, …, T. Misteli. 2004. Global nature of dynamic protein-chromatin interactions in vivo: three-dimensional genome scanning and dynamic interaction networks of chromatin proteins. *Mol. Cell. Biol.* 24:6393–6402.
3. Köster, M., T. Frahm, and H. Hauser. 2005. Nucleocytoplasmic shuttling revealed by FRAP and FLIP technologies. *Curr. Opin. Biotechnol.* 16:28–34.
4. Braga, J., J. G. McNally, and M. Carmo-Fonseca. 2007. A reaction-diffusion model to study RNA motion by quantitative fluorescence recovery after photobleaching. *Biophys. J.* 92:2694–2703.
5. Carrero, G., E. Crawford, …, M. J. Hendzel. 2004. Quantification of protein-protein and protein-DNA interactions in vivo, using fluorescence recovery after photobleaching. *Methods Enzymol.* 375:415–442.
6. Stavreva, D. A., and J. G. McNally. 2004. Fluorescence recovery after photobleaching (FRAP) methods for visualizing protein dynamics in living mammalian cell nuclei. *Methods Enzymol.* 375:443–455.
7. Giese, B., C.-K. Au-Yeung, …, G. Müller-Newen. 2003. Long term association of the cytokine receptor gp130 and the Janus kinase Jak1 revealed by FRAP analysis. *J. Biol. Chem.* 278:39205–39213.
8. Howell, B. J., D. B. Hoffman, …, E. D. Salmon. 2000. Visualization of Mad2 dynamics at kinetochores, along spindle fibers, and at spindle poles in living cells. *J. Cell Biol.* 150:1233–1250.
9. Howell, B. J., B. Moree, …, E. D. Salmon. 2004. Spindle checkpoint protein dynamics at kinetochores in living cells. *Curr. Biol.* 14: 953–964.
10. Sprague, B. L., R. L. Pego, …, J. G. McNally. 2004. Analysis of binding reactions by fluorescence recovery after photobleaching. *Biophys. J.* 86:3473–3495.
11. Carrero, G., E. Crawford, …, G. de Vries. 2004. Characterizing fluorescence recovery curves for nuclear proteins undergoing binding events. *Bull. Math. Biol.* 66:1515–1545.
12. Carrero, G., D. McDonald, …, M. J. Hendzel. 2003. Using FRAP and mathematical modeling to determine the in vivo kinetics of nuclear proteins. *Methods.* 29:14–28.
13. Reits, E. A., and J. J. Neefjes. 2001. From fixed to FRAP: measuring protein mobility and activity in living cells. *Nat. Cell Biol.* 3:E145–E147.
14. Houtsmuller, A. B., and W. Vermeulen. 2001. Macromolecular dynamics in living cell nuclei revealed by fluorescence redistribution after photobleaching. *Histochem. Cell Biol.* 115:13–21.
15. White, J., and E. Stelzer. 1999. Photobleaching GFP reveals protein dynamics inside live cells. *Trends Cell Biol.* 9:61–65.
16. Morris, M. D. 1991. Factorial sampling plans for preliminary computational experiments. *Technometrics.* 33:161–174.
17. Saltelli, A., M. Ratto, …, S. Tarantola. 2008. Global Sensitivity Analysis. The Primer. John Wiley & Sons, New York.
18. Mai, J., S. Trump, …, S. Attinger. 2011. Are assumptions about the model type necessary in reaction-diffusion modeling? A FRAP application. *Biophys. J.* 100:1178–1188.
19. Hinow, P., C. E. Rogers, …, E. DiBenedetto. 2006. The DNA binding activity of p53 displays reaction-diffusion kinetics. *Biophys. J.* 91: 330–342.
20. Mueller, F., P. Wach, and J. G. McNally. 2008. Evidence for a common mode of transcription factor interaction with chromatin as revealed by improved quantitative fluorescence recovery after photobleaching. *Biophys. J.* 94:3323–3339.
21. Ekstrom, P.E. 2005. Eikos- A Simulation Toolbox for Sensitivity Analysis. Global Sensitivity Analysis (software). The European Commission Joint Research Center, Ispra, Italy. http://sensitivity-analysis.jrc.ec.europa.eu.
22. Campolongo, F., J. Cariboni, and A. Saltelli. 2007. An effective screening design for sensitivity analysis of large models. *Environ. Model. Softw.* 22:1509–1518.
23. Weiss, M. 2004. Challenges and artifacts in quantitative photobleaching experiments. *Traffic.* 5:662–671.
24. Olveczky, B. P., and A. S. Verkman. 1998. Monte Carlo analysis of obstructed diffusion in three dimensions: application to molecular diffusion in organelles. *Biophys. J.* 74:2722–2730.
25. Sbalzarini, I. F., A. Mezzacasa, …, P. Koumoutsakos. 2005. Effects of organelle shape on fluorescence recovery after photobleaching. *Biophys. J.* 89:1482–1492.
26. Sbalzarini, I. F., A. Hayer, …, P. Koumoutsakos. 2006. Simulations of (an)isotropic diffusion on curved biological surfaces. *Biophys. J.* 90:878–885.
27. Siggia, E. D., J. Lippincott-Schwartz, and S. Bekiranov. 2000. Diffusion in inhomogeneous media: theory and simulations applied to whole cell photobleach recovery. *Biophys. J.* 79:1761–1770.
28. Saxton, M. J. 2001. Anomalous subdiffusion in fluorescence photobleaching recovery: a Monte Carlo study. *Biophys. J.* 81:2226–2240.
29. Koumoutsakos, P. 2005. Multiscale flow simulations using particles. *Annu. Rev. Fluid Mech.* 37:457–487.
30. Angelides, K. J., L. W. Elmer, …, E. Elson. 1988. Distribution and lateral mobility of voltage-dependent sodium channels in neurons. *J. Cell Biol.* 106:1911–1925.
31. Broser, P. J., R. Schulte, …, G. Wittum. 2004. Nonlinear anisotropic diffusion filtering of three-dimensional image data from two-photon microscopy. *J. Biomed. Opt.* 9:1253–1264.
32. Jungblut, D., G. Queisser, and G. Wittum. 2011. Inertia based filtering of high resolution images using a GPU cluster. *Comp. Vis. Sci.* 14:181–186.

Parameter Importance in FRAP Acquisition and Analysis: A Simulation Approach

Juliane Mai[*] [§] Saskia Trump[†] Irina Lehmann[†]

Sabine Attinger [*‡]

[*]Department of Computational Hydrosystems, UFZ - Helmholtz Centre for Environmental Research, Leipzig, Germany

[†]Department of Environmental Immunology, UFZ - Helmholtz Centre for Environmental Research, Leipzig, Germany

[‡]Institute for Geosciences, University of Jena, Jena, Germany

[§]Corresponding author. Address: Department of Computational Hydrosystems, UFZ - Helmholtz Centre for Environmental Research, Permoser Straße 15, 04318 Leipzig, Leipzig, Germany, Tel.: +49 341 2351250, Fax: +49 341 2351939, juliane.mai@ufz.de

Supplementary Material

1 Computational Specifications

The Monte-Carlo simulations were run as batch jobs on single nodes of our cluster (Dual socket Six-Core Intel Xeon X5650 processors with 64 GB physical RAM). Each simulation was performed using $a = 10,000$ samples, $b = 1,000$ time steps and $c = 10$ simulation runs which were averaged in order to generate smooth recovery curves.
The mean processing time $\overline{t}$ of the various simulations are given in the following:

(I) IC: $\overline{t} = 38.9s$

(II) BC: $\overline{t} = 51.6s$

(III) Position: $\overline{t} = 1858.0s$

The algorithmic complexity of all scenarios is $O(n^3) = O(a) \cdot O(b) \cdot O(c)$.

2 Diffusion

The undirected movement of particles in liquids or gas is called diffusion or *Brownian* motion. To model a *Brownian* motion one *Gaussian* distributed random number $d_i \sim N[\mu, \sigma]$ for each spatial direction i has to be generated (1). The mean μ of an unbiased diffusion process is equal to zero while the standard deviation σ is dependent on the diffusion coefficient D of the simulated particle and the time step Δt used for simulation

$$\sigma \quad = \quad \sqrt{2D\Delta t} \quad .$$

For each spatial direction i and particle $k = 1 \ldots N$ such a random number has to be produced. The new particle position $x_i(t + \Delta t)$is then calculated by adding these numbers to the previous position $x_i(t)$ of the particle.

3 Reaction

In general, networks of reacting molecules consist of two different basic structures: Either (I) a molecule has different possibilities to convert (A $\rightarrow$ B or A $\rightarrow$ C) or (II) molecules react sequentially (A $\rightarrow$ B $\rightarrow$ C). This two types of connections lead to different equations describing the reactive network. Therefore, the type of connection is important and has to be fixed when modeling such networks.

In modeling FRAP data traditionally, the molecule of interest is allowed to convert following type (I), i.e. the molecule may undergo S different binding reactions with other substances. Each reaction is described by

$$F + V_\mathrm{i} \underset{k_{\mathrm{off_i}}}{\overset{k_{\mathrm{on_i}}}{\rightleftharpoons}} B_\mathrm{i} \qquad , \quad \mathrm{i} = 1 \ldots \mathrm{S} \quad . \tag{S.1}$$

The unbound (free) fraction of molecules F binds with V_i vacant binding sites to form the bound fraction of molecules B_i. $k_{\mathrm{on_i}}$ and $k_{\mathrm{off_i}}$ are the corresponding association and dissociation rates in $[\mathrm{mol} \cdot s^{-1}]$ and $[s^{-1}]$, respectively. Since all reactions are dependent on the free fraction F the reaction network can be illustrated as a star-like scheme where F is located in the center surrounded by B_i. Therefore, this kind of reaction scheme will be denoted as *star structure reaction*. Further information, on modeling this type of reactive coupling can be found in Sprague et al. (2).
Unlike the reactions (Eq. S.1) where all bound states B_i depend directly on the free fraction F, a more realistic scenario is to model *reactions as a chain*

$$B_{\mathrm{i\text{-}1}} + V_\mathrm{i} \underset{k_{\mathrm{off_i}}}{\overset{k_{\mathrm{on_i}}}{\rightleftharpoons}} B_\mathrm{i} \qquad , \quad \mathrm{i} = 1 \ldots \mathrm{S} \tag{S.2}$$

where B_0 represents the free molecular fraction F. An example of such a scheme in the case of three binding states is given in Eq. S.3.

$$F = B_0 \underset{k_{\mathrm{off}_1}}{\overset{k_{\mathrm{on}_1}}{\rightleftharpoons}} B_1 \underset{k_{\mathrm{off}_2}}{\overset{k_{\mathrm{on}_2}}{\rightleftharpoons}} B_2 \underset{k_{\mathrm{off}_3}}{\overset{k_{\mathrm{on}_3}}{\rightleftharpoons}} B_3 \tag{S.3}$$

This reaction scheme is more realistic if a special consecutive binding of molecules, i.e. C can only bind to A if B has already bound to A, is needed before the complex of $A + B + C$ can bind. This kind of restrictions are commonly needed to describe biological processes.
This chain reaction scheme leads to modified differential equations and equilibrium concentrations as described by Mai et al. (3). These two reaction schemes necessitate different implementations, which are implemented as follows.

3.1 Implementation of a star structure reaction

The equilibrium concentrations F_eq and B_{eq_i} of the modeled fractions F and B_i can be found in Mai et al. (3) (Eq. 7) and are used to set the initial binding state $BS_{i=1\ldots N}$ of N molecules. For example, in presence of three fractions of molecules ($F_\mathrm{eq} = 10\%$, $B_{\mathrm{eq}_1} = 30\%$, and $B_{\mathrm{eq}_2} = 60\%$) and a

reaction simulation of $N = 10,000$ molecules, the first $1,000$ molecules will be set to $BS = 0$. Subsequent, the next $3,000$ molecules are set to binding state $BS = 1$ and the last $6,000$ molecules in binding state $BS = 2$. Hence, all free molecules are in binding state $BS = 0$ and bound molecules have the binding state $BS \geq 1$.
For each simulated time step $t = 1 \dots T$ and molecule $k = 1 \dots N$ a uniform distributed random number $r \sim [0, 1)$ is generated. This random number r afterwards is used to decide whether a molecule will change its binding state or not.

Change from bound to free state: A bound molecule ($BS(t) = i$) at time step t either changes to the unbound state $BS(t + \Delta t) = 0$ or remains in its bound state $BS(t + \Delta t) = i$. The probability of change depends on the dissociation rate $k_{\mathrm{off_i}}$. To calculate that dependency one has to solve the ordinary differential equation describing the dissociation process using the equilibrium concentration as an initial condition:

$$\frac{\partial c_{\mathrm{B_i}}}{\partial t} = -k_{\mathrm{off_i}} c_{\mathrm{B_i}} \quad , \quad \mathrm{i} = 1 \dots \mathrm{S} \tag{S.4a}$$

$$c_{\mathrm{B_i}}(0) = B_{\mathrm{eq}_i} \tag{S.4b}$$

The solution of that equation is determined by

$$c_{\mathrm{B_i}}(t) = B_{\mathrm{eq}_i} \cdot e^{-k_{\mathrm{off}_i} t} \quad , \quad \mathrm{i} = 1 \dots \mathrm{S} \tag{S.5}$$

Therefore, the probability that a bound molecule stays bound for a time Δt is equal to $e^{-k_{\mathrm{off}_i} \Delta t}$ whereas the probability of a change to the free state is equal to $1 - e^{-k_{\mathrm{off}_i} \Delta t}$. The determination of the new binding states is implemented as follows:

```
# bound molecules (BS = i :  i > 0)
do t = 1, T
    do k = 1, N
       r = DRNUNF()                    # r ~ [0,1)
       if (r ≤ 1 − e^(−k_off_i · Δt)) then
          BS(k) = 0
       else
          BS(k) = i
    end do
end do
```

Change from free to bound state: A free molecule ($BS(t) = 0$) at time step t has the possibility to stay in the free state $BS(t + \Delta t) = 0$ or to switch over to a bound state $BS(t + \Delta t) \geq 1$ at $t + \Delta t$. The probability to change to the binding state $BS = i$ depends on the association rate $k_{\mathrm{on_i}}$ and dissociation rate $k_{\mathrm{off_i}}$.
The amount A of particles changing from bound state to free state is the sum of all bound fractions multiplied by the percentage of change

$$A = \sum_{i}^{S} \underbrace{\left(1 - e^{-k_{\mathrm{off}_i} \Delta t}\right)}_{\substack{\text{probability of change from} \\ \text{bound state (BS=i) to free} \\ \text{state (BS=0)}}} \cdot B_{\mathrm{eq}_i} \tag{S.6}$$

Since the equilibrium condition has to be fulfilled, i.e. the sum of particles is constant, A has to be equal for the bound as well as for the free state. Therefore, inserting the equation given for the equilibrium concentration of bound molecules B_{eq_i} (Mai et al. (3): Eq. 7) leads to

$$A = \sum_{i}^{S} \underbrace{\left(1 - e^{-k_{\mathrm{off}_i} \Delta t}\right) \cdot \frac{k_{\mathrm{on}_i}}{k_{\mathrm{off}_i}}}_{\substack{\text{probability of change from} \\ \text{free state (BS=0) to bound} \\ \text{state (BS=i)}}} \cdot F_{\mathrm{eq}_i} \tag{S.7}$$

It is easy to perceive the probability of a change from free to bound state as part of this equation.

```
# free molecules (BS = 0)
do t = 1, T
    do k = 1, N
       r = DRNUNF()                    # r ~ [0,1)
       if (r ≤ k_on1/k_off1 · (1 − e^(−k_off1·Δt))) then
          BS(k) = 1
       else
          if (r ≤ k_on1/k_off1 · (1 − e^(−k_off1·Δt)) + k_on2/k_off2 · (1 − e^(−k_off2·Δt))) then
             BS(k) = 2
          else
             ...
    end do
end do
```

3.2 Implementation of a chain structure reaction

The equilibrium concentrations B_{eq_i} of the modeled fractions B_i were introduced by Mai et al. (3) (Eq. 12) and are used to set the initial binding state BS of N molecules in the same way as already described above for the star structure reaction.
In the next sections the implementation of the *chain structure reaction*, i.e. the change from molecules in the first to the intermediate or the final state respectively, will be described. The definition of the different kinds of states is illustrated in Eq. S.8.

$$\underbrace{B_0}_{\text{first state}} \underset{k_{\mathrm{off}_1}}{\overset{k_{\mathrm{on}_1}}{\rightleftharpoons}} \underbrace{B_1 \underset{k_{\mathrm{off}_2}}{\overset{k_{\mathrm{on}_2}}{\rightleftharpoons}} \dots \underset{k_{\mathrm{off}_{\text{S-1}}}}{\overset{k_{\mathrm{on}_{\text{S-1}}}}{\rightleftharpoons}} B_{\text{S-1}}}_{\text{intermediate state}} \underset{k_{\mathrm{off}_\mathrm{S}}}{\overset{k_{\mathrm{on}_\mathrm{S}}}{\rightleftharpoons}} \underbrace{B_\mathrm{S}}_{\text{final state}} \tag{S.8}$$

Change of molecules in first state (BS = 0): A free molecule ($BS(t) = 0$) at time step t either changes to the first bound state $BS(t + \Delta t) = 1$ or remains in its current state. The probability to change depends on the association rate k_{on_1} and on the dissociation rate k_{off_1}. The dependency is the same as described in Eq. S.7.

```
# free molecules (BS = 0)
do t = 1, T
    do k = 1, N
       r = DRNUNF()                          # r ~ [0,1)
       if (r ≤ (k_on_1 / k_off_1) · (1 − e^(−k_off_1 · Δt))) then
          BS(k) = 1
       else
          BS(k) = 0
    end do
end do
```

Change of molecules in final state (BS = S): A molecule in the final binding state ($BS(t) = S$) at time step t either changes to the previous bound state $BS(t + \Delta t) = S - 1$ or remains in its current state. The probability to change depends on the dissociation rate $k_{\mathrm{off}_\mathrm{S}}$. The dependency is the same as described in Eq. S.6.

```
# final bound state molecules (BS = S)
do t = 1, T
    do k = 1, N
       r = DRNUNF()                    # r ~ [0,1)
       if (r ≤ (1 − e^(−k_offS·Δt))) then
          BS(k) = S - 1
       else
          BS(k) = S
    end do
end do
```

Change of molecules in intermediate state ($\mathbf{0 < BS < S}$): Molecules in an intermediate binding state ($BS(t) = i$, $0 < i < S$) at time step t either changes to the previous ($BS(t + \Delta t) = i - 1$) or to the next bound state ($BS(t + \Delta t) = i + 1$) or remain in their current state. The probability to change depends on the association rate $k_{\mathrm{on_{i+1}}}$ as well as on the dissociation rates $k_{\mathrm{off_i}}$ and $k_{\mathrm{off_{i+1}}}$. The dependency is the same as described in Eq. S.6 and Eq. S.7.

```
# intermediate bound state molecules (BS = i :  0 < i < S)
do t = 1, T
    do k = 1, N
       r = DRNUNF()                    # r ~ [0,1)
       if (r ≤ (1 − e^(−k_offi·Δt))) then
          BS(k) = i - 1
       else
          if (r ≤ (1 − e^(−k_offi·Δt)) + (k_oni+1 / k_offi+1) · (1 − e^(−k_offi+1·Δt))) then
             BS(k) = i + 1
          else
             BS(k) = i
    end do
end do
```

4 Geometries

In order to perform particle simulations in complex geometries certain boundaries have to be considered. In the given case such boundaries constitute cellular membranes including different intracellular substructures (i.e. or-

ganelles).
Depending on their compartmental localization the particles may have different properties. Diffusion coefficients for example differ depending on the heterogeneous viscosity of the cellular matrix. Therefore, at each simulation time step it is necessary to determine the actual position, including the subcellular structure, for each particle.
For simple geometries that have an analytical description, like a circle (e.g. the bleaching spot) with a radius r and its center (x_M, y_M), the particle assignment is implemented using the following equation:

$$(x - x_M)^2 + (y - y_M)^2 \leq r^2 \quad . \tag{S.9}$$

However, for more complex geometries (e.g. cytoplasm or the nucleus) where a finite element surface mesh (polygonal line) is given, the implementation of the *Point Inclusion in Polygon Test* (*PNPOLY*) by W. Randolph Franklin is used for the 2D simulations. The aim of this method is to assign the position of a particle outside or inside of a polygon. The basic idea is to define a semi-infinite ray starting at the particle's position and counting the intersections of this ray with the polygon. Since at every crossing there is a switch from the inner to the outer area of the polygon (*Jordan curve theorem*), the number of intersections can be used to assign the particle to the inside or outside of the polygon. The original source code by W. Randolph Franklin is accessible via `www.ecse.rpi.edu/Homepages/wrf/Research/Short_Notes/pnpoly.html`. Since this source code insufficiently assigns the vertex/edge property to some particles the code was adapted accordingly. The result of a toy example comparing the original versus the adapted source code are shown in Fig. S.1.
As shown in Fig. S.1(A) the original source code insufficiently assigns the vertex/edge property to some particles. The particles on the edges as well as the particles on vertical and horizontal vertexes are not assigned correctly. Therefore, the code was adapted as shown below where comments are highlighted in gray and added lines are highlighted in blue. The correction for particles on edges is done in line 11 while the particle's position on vertical and horizontal vertexes are corrected in lines 15-18 and lines 19-22, respectively.

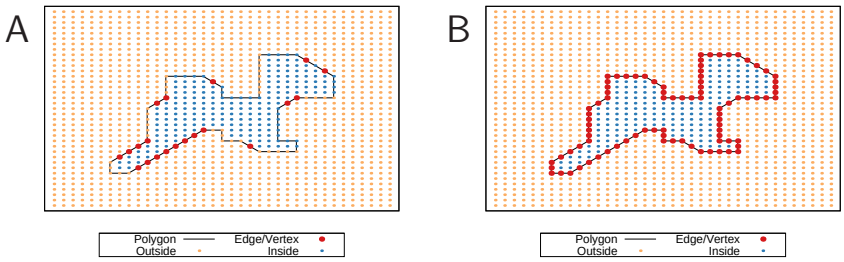

Figure S.1: The results of location assignment for particles using a toy polygon are presented. (A) shows the assignment using the original `PNPOLY` algorithm where the positions on the border of the polygon were not assigned correctly while (B) shows the results of the adapted `PNPOLY` algorithm with the correct assignment of boundary positions.

```
01 SUBROUTINE PNPOLY(PX,PY,XX,YY,N,INOUT)
# DESCRIPTION OF THE PARAMETERS
#    PX/PY    - X/Y-COORDINATE OF POINT IN QUESTION.
#    XX/YY    - N LONG VECTOR CONTAINING X/Y-COORDINATES OF
#                  VERTEXES OF POLYGON.
#    N         - NUMBER OF VERTEXES IN THE POLYGON.
#    INOUT    - THE SIGNAL RETURNED:
#                     -1 IF THE POINT IS OUTSIDE OF THE POLYGON,
#                      0 IF THE POINT IS ON AN EDGE OR AT A VERTEX,
#                      1 IF THE POINT IS INSIDE OF THE POLYGON.
02 REAL X(2000),Y(2000),XX(N),YY(N)
03 LOGICAL MX,MY,NX,NY
04 MAXDIM=2000
05     IF(N.LE.MAXDIM) GOTO 6
06     PRINT *,'WARNING:',N,' TOO GREAT. RESULTS INVALID')
07     RETURN
...
```

```
08 6   DO 1 I=1,N
09        X(I)=XX(I)-PX
10        Y(I)=YY(I)-PY
11 1      IF((X(I).EQ.0.0).AND.(Y(I).EQ.0.0)) GOTO 4   #Edge
12     INOUT=-1
13     DO 2 I=1,N
14        J=1+MOD(I,N)
15        IF( (XX(I).EQ.XX(J)).AND.(XX(I).EQ.PX) ) THEN   # vert. Vertex
16           LY=(PY-YY(J))/(YY(I)-YY(J))
17           IF((LY.GE.0.0).AND.(LY.LE.1.0) ) GOTO 4
18        ENDIF
19        IF( (YY(I).EQ.YY(J)).AND.(YY(I).EQ.PY) ) THEN   # hor. Vertex
20           LX=(PX-XX(J))/(XX(I)-XX(J))
21           IF((LX.GE.0.0).AND.(LX.LE.1.0) ) GOTO 4
22        ENDIF
23        MX=X(I).GE.0.0
24        NX=X(J).GE.0.0
25        MY=Y(I).GE.0.0
26        NY=Y(J).GE.0.0
27        IF(.NOT.((MY.OR.NY).AND.(MX.OR.NX)).OR.(MX.AND.NX)) GOTO 2
28        IF(.NOT.(MY.AND.NY.AND.(MX.OR.NX).AND..NOT.(MX.AND.NX))) GOTO 3
29        INOUT=-INOUT
30        GOTO 2
31 3      IF((Y(I)*X(J)-X(I)*Y(J))/(X(J)-X(I))) 2,4,5
32 4      INOUT=0
33        RETURN
34 5      INOUT=-INOUT
35 2   CONTINUE
36     RETURN
37     END
```

5 Boundary Condition

The next step after determining the compartment location of each particle is to implement appropriate boundary conditions.
A "no flow"-boundary conditions was implemented to address the case that particles are not allowed or hindered to leave a particular cellular compartment. The implementation of this condition is based on particle reflection (4). For this purpose the position of particles crossing a "no flow"-boundary has to be determined and recalculated. The calculation of the new position is applied as long as the position of the particle is outside of the polygon. Addressing the exception that no position can be found inside the polygon after 10 recalculations, the particle is set to a random position inside the polygon in order to avoid infinite loops.
In case of an analytical geometry, i.e. a circle (Eq. S.9), a simplified strategy is used for the "no flow"-condition implementation. Therefore, the coordinates for the circle and the particle position $(x^{\text{out}}, y^{\text{out}})$ have to be transformed such that the center of the circle is the point of origin.
The basic concept is to mirror the initial position $(x^{\text{out}}, y^{\text{out}})$ to the other side of the circle $(-x^{\text{out}}, -y^{\text{out}})$ and subtract a vector with direction to the point of origin and a norm of $2r$ to determine the new position $(x^{\text{in}}, y^{\text{in}})$.

6 Initial Condition

The bleaching spot profile observed directly after bleaching corresponds to a *Gaussian* distribution. However, calculating an analytical solution for such a scenario is not possible in most cases. Nevertheless, methods have been described how to simplifying the initial *Gaussian* condition to make calculating an analytical solution possible.
The following section will describe how to stepwise generate a constant initial value such that it sufficiently represents the *Gaussian* case by adapting a method previously described by Hinow et al. (5). Consecutively, (1) a *Gaussian* function has to be fitted to the data, (2) the constant initial value θ has to be calculated, and (3) the radius r_0 used for the original FRAP experiment has to be adapted to R.
Subsequently, the method and mathematical background to determine the radius and initial value will be described. Initially, a *Gaussian* function (Eq. S.10) is fitted to the measured bleaching spot profile (Fig. S.2(A)). The fitted parameters are a and σ.

$$I(r) \quad = \quad 1 - (1 - a) \cdot \exp\left(-\frac{r^2}{2\sigma^2}\right) \tag{S.10}$$

Afterwards, the fitted intensity profile $I(r)$ is used to determine a constant initial value θ such that the bleached fraction within the bleaching spot equals the area limited by θ (Fig. S.2(B)). Therefore, the radius r_0 of the bleaching spot is required. Since r_0 is the original radius of the spot used for performing the FRAP experiment, it is known. θ is determined by Eq. S.11. There, the radius r_0 is fixed while the constant value θ is adjusted.

$$\theta = \frac{2}{r_0^2} \int_0^{r_0} r \cdot I(r)\, dr \tag{S.11}$$

To conserve the amount of unbleached molecules, the bleaching spot radius also has to be inverted. The adapted radius R is determined by the area limited by $(1-\theta)$ and R which equals the fraction of unbleached molecules (Fig. S.2(C)). This fraction is described by $1 - I(r)$. The adapted radius R is determined by Eq. S.12. Here, the constant value θ is fixed while the radius R is adjusted.

$$R = \sqrt{\frac{2}{1-\theta} \cdot \int_0^{\infty} r \cdot [1 - I(r)]\, dr} \tag{S.12}$$

The method described is to simplify the *Gaussian* distribution within the bleaching spot after bleaching by a constant initial value. Therefore, not only the initial value has to be adapted but also the radius of the bleaching spot has to be adjusted. The ability of this strategy to describe the *Gaussian* profile by such a constant value requires simulations using a *Gaussian* initial condition, since an analytical solution of this case is not available.

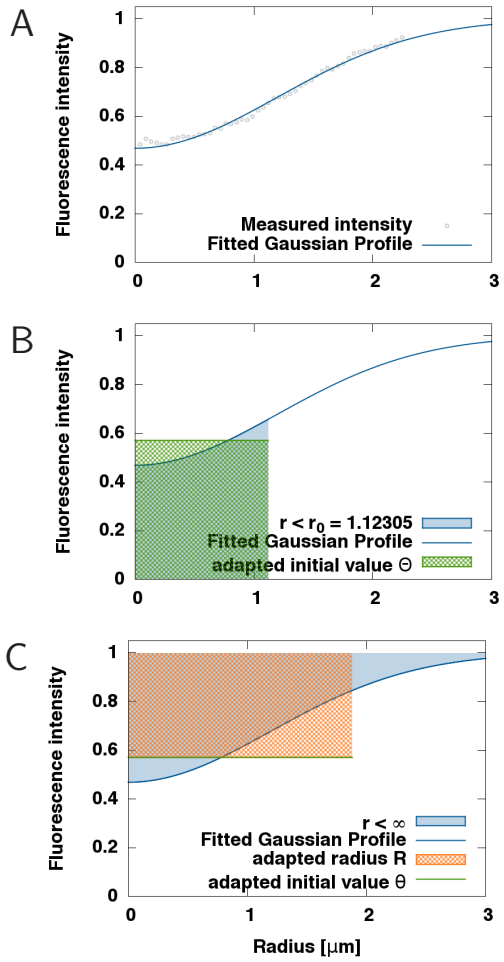

Figure S.2: Stepwise adaption of the initial constant value θ and bleaching spot radius R. (A) Fitting a *Gaussian* profile to measured bleaching spot profile (blue line) to measurements (gray dots) using Eq. S.10. (B) Determination of a constant initial value θ (height of green box) such that the experimentally bleached amount described by a *Gaussian* curve (blue area) equals the bleached amount using a constant value (green box) within the original bleaching spot with radius r_0 (Eq. S.11). (C) Determination of adapted radius R such that the total amount of (experimentally) unbleached amount (blue area) equals the unbleached amount set by the constant initial condition (red box) using Eq. S.12.

7 Influence of bleaching spot position

The bleaching spot positioning was studied within complex geometries. The simulation setup, the resulting recovery curves, the distribution of the bleached particles at the end of simulation are shown in Fig. S.3. To address the relative position of the bleaching spot to the compartment boundary, we introduce a new parameter d_M which represents the mean distance to the periphery. d_M is calculated as the mean length of 60 line segments from the bleaching spot center to the geometry boundary. This distance measure yields small values for positions in cell edge protrusions and comparable large values for positions near a halfplane (Fig. S.3: Spot 3) as well as in the center of the geometry (Fig. S.3: Spot 1). The distribution of the distance measure d_M within the cytoplasmic geometry and an example of the derivation of d_M are depicted in Fig. S.3(G) and Fig. S.3(H) respectively.

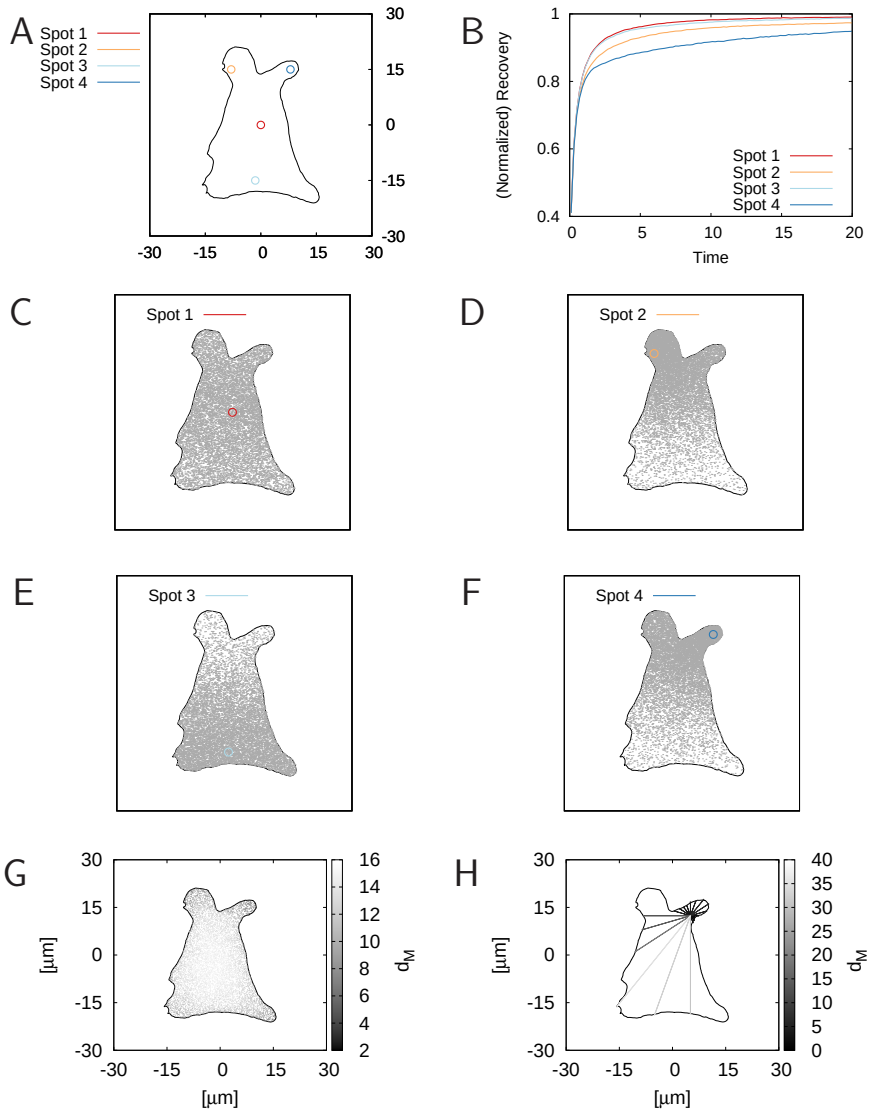

Figure S.3: FRAP experiments simulated at different positions within a real 2D cell geometry (A), give rise to diverse recovery curves (B) and different distributions of bleached particles at the end of simulation (C-F). A distance measure of the bleaching spot center relative to the domain boundary is applied such that positions in protrusions are overall closer to the membrane than central positions (G). The distance d_M equals the mean length of 60 line segments from the bleaching spot center to the geometry boundary (H).

8 Sub-/ Super-Diffusion

Effect of sub- & super-diffusion processes. The simulations performed so far were based on a *Brownian* motion. In real cellular environments this might not be applicable. On one hand molecular crowding in the cytoplasm is known to influence diffusion processes. The classic diffusion is converted to an anomalous sub-diffusion. On the other hand directed transport processes can be approximated by an anomalous super-diffusion.
Anomalous diffusion processes are characterized by a non-linear relationship between time and the mean square displacement of a particle $\langle x^2 \rangle$. Often a power-law is used to describe this non-linear relationship: $\langle x^2 \rangle \propto t^\alpha$. The exponent α determines the type of diffusion: $\alpha = 1$ for typical diffusion, $\alpha < 1$ for sub-diffusion, and $\alpha > 1$ in case of super-diffusion.
In order to study the effect of an unknown exponent α, we performed simulations and calculated the *Elementary Effect* of anomalous diffusion processes. The Elementary Effects are shown in Fig. S.4. The parameter used can be found in Tab. 1 and 2, parameter ranges $\mathrm{III_B}$. The parameter range of α was set to $[0.5, 1.5]$.
As depicted in Fig. S.4(a) to reliably invert all reaction-diffusion parameters the *Elementary Effects* of the experimental setup parameters would have to be below the one observed for D_1. Suggesting that the parameter ranges have to be reduced. However, if there is a considerable sub-/super-diffusion restricting the experimental parameter ranges would not be sufficient to invert D_1 reliably, since the *Elementary Effect* of α is still above the one observed for D_1 (Fig. S.4(b)). Only in case of a known α for the system observed, minimizing the ranges for the experimental parameters would allow for inverting the reaction-diffusion parameters accurately.

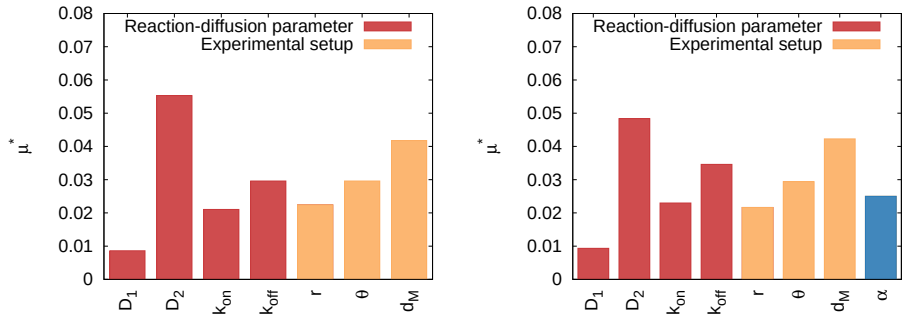

(a) normal diffusion $\alpha = 1$ (b) anomalous diffusion $\alpha \in [0.5, 1.5]$

Figure S.4: Effect of sub- & super-diffusion processes.

9 Projection Errors of 3D Processes

The simplification of 3D processes by 2D models particularly influences the *Elementary Effects* of the experimental parameters r, θ, and d_M (Fig. S.5). All of these *Elementary Effects* are decreased compared to the 2D case. Reducing the experimental parameter ranges based on the 2D *Elementary Effects* will in any case result in lower 3D *Elementary Effects* of these parameters. Therefore, reducing the *Elementary Effects* of the experimental parameters below those of the reaction-diffusion parameters based on the 2D results will certainly allow a reliable inversion of the reaction-diffusion parameters.

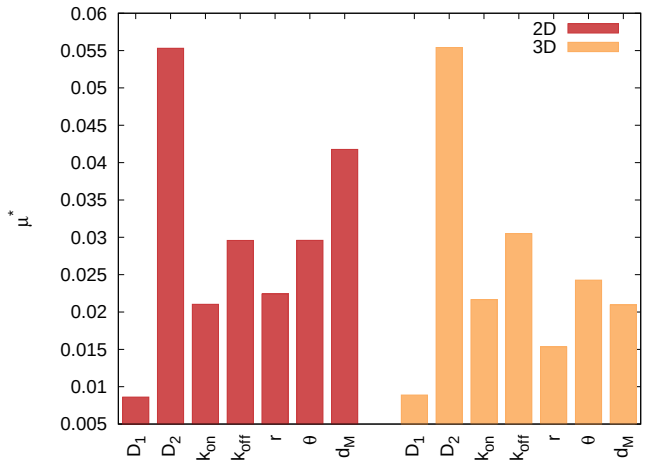

Figure S.5: Effect of projection errors of 3D processes.

References

1. Berg, H. C., 1993. Random Walks in Biology. Princeton University Press.

2. Sprague, B. L., R. L. Pego, D. A. Stavreva, and J. G. McNally, 2004. Analysis of Binding Reaction by Fluorescence Recovery after Photobleaching. Biophys. J. 86:3473–3495.

3. Mai, J., S. Trump, R. Ali, R. L. Schiltz, G. Hager, T. Hanke, I. Lehmann, and S. Attinger, 2011. Are assumptions about the model type necessary in reaction diffusion modeling?- A FRAP application. Biophys. J. 100:1178–1188.

4. Kerr, R. A., T. M. Bartol, B. Kaminsky, M. Dittrich, J.-C. J. Chang, S. B. Baden, T. J. Sejnowski, and J. R. Stiles, 2008. Fast Monte Carlo Simulation Methods for Biological Reaction-Diffusion Systems in Solution and on Surfaces. SIAM J Sci Comput 30:3126.

5. Hinow, P., C. E. Rogers, C. E. Barbieri, J. A. Pietenpol, A. K. Kenworthy, and E. DiBenedetto, 2006. The DNA binding activity of p53 displays reaction-diffusion kinetics. Biophys. J. 91:330–342.